ELSEVIER

Contents lists available at ScienceDirect

## International Journal of Heat and Mass Transfer

journal homepage: www.elsevier.com/locate/hmt



# Anisotropically tuning interfacial thermal conductance between graphite and poly(ethylene oxide) by lithium-ion intercalation: A molecular dynamics study



Siyu Tian<sup>a</sup>, Zhihao Xu<sup>b</sup>, Shiwen Wu<sup>a</sup>, Tengfei Luo<sup>b,\*</sup>, Guoping Xiong<sup>a,\*</sup>

- <sup>a</sup> Department of Mechanical Engineering, The University of Texas at Dallas, 800 W Campbell Rd, Richardson, TX 75080, United States
- <sup>b</sup> Department of Aerospace and Mechanical Engineering, University of Notre Dame, Notre Dame, IN 46556, United States

#### ARTICLE INFO

Article history:
Received 4 March 2022
Revised 26 May 2022
Accepted 8 June 2022
Available online 19 June 2022

Keywords: Graphite/polymer composites Lithium-ion intercalation Thermal transport Molecular dynamics

#### ABSTRACT

Understanding interfacial thermal transport between lithiated two-dimensional materials and polymers can provide useful guidelines to design thermally tunable and conductive composites for efficient thermal management of energy systems. In this work, molecular dynamics simulations are conducted to investigate the effect of lithium (Li)-ion intercalation on the interfacial thermal transport between graphite and poly(ethylene oxide) (PEO). Results show that Li-ion intercalation anisotropically affects the enhancement of the interfacial thermal conductance (ITC) between graphite and PEO. The cross-plane ITC monotonically increases with increasing degree of lithiation, while a significant enhancement of the in-plane ITC is only observed when the graphite host is fully lithiated. The anisotropic effect can be attributed to the intercalation-induced strong Lennard-Jones interactions between the two contacting materials. This work may open up new opportunities to design thermally conductive polymeric composites and thermally controllable interfaces through ion intercalation of 2D materials.

© 2022 Elsevier Ltd. All rights reserved.

## 1. Introduction

Polymeric composites with superior thermal properties have been widely used for thermal management in electronics and energy storage/conversion systems because of the growing risks of thermal-related issues (e.g., thermal runaway, overheating) in these devices [1,2]. Because of the high thermal conductivity of graphite, the thermal conductivity of polymeric composites can be significantly improved by using graphite as a filler material [3]. Although extensive research has been conducted to design thermally conductive graphite/polymer composites, the thermal conductivity of such composites is still far below expectation [4]. These unsatisfactory results can be partially attributed to the high interfacial thermal resistance (or Kapitza resistance) between the graphite fillers and the polymer matrix [5,6]. Therefore, it is of great importance to understand the thermal transport across graphite/polymer interfaces for designing thermally conductive polymeric composites.

To date, many approaches have been reported to control the thermal transport in bulk materials and the thermal transport across interfaces, including hybridization [7], electric-field modulation [8], structure poling [9], covalent bonding [10,11], inter-

E-mail addresses: tluo@nd.edu (T. Luo), guoping.xiong@utdallas.edu (G. Xiong).

face modification [12], interlayer rotation [13], and functionalization [14-16]. Among them, many approaches can effectively increase interfacial thermal conductance (ITC). However, tuning the thermal transport between two contacting materials dynamically and reversibly seems rather challenging for the thermal management of energy systems. Recent experimental studies have shown that the thermal conductivity of 2D materials (e.g., MoS<sub>2</sub>, black phosphorus) can be electrochemically tuned by Li-ion intercalation [17,18]. For instance, Zhu et al. measured the thermal conductivity of MoS<sub>2</sub> using time-domain thermoreflectance and showed that the thermal anisotropy ratio in bulk MoS<sub>2</sub> crystals can be electrochemically tuned from 52 to 110 by changing the concentration of intercalated Li ions [17]. The thermal transport properties of lithiated graphite have also been studied by MD simulations [19-21]. The electrochemical intercalation of Li ions into graphite is reversible and controllable, which follows the redox reaction:  $xLi^+ + xe^- + C_6 \leftrightarrow Li_xC_6$ , where  $C_6$  represents the graphite host, and the lithiation degree x ranges from 0 to 1 depending on the charge/discharge state [22,23]. Such an electrochemical intercalation strategy may also be applicable to tune the interfacial thermal transport between 2D materials and polymers. Although previous MD studies have shown that the thermal transport across graphite/Al and graphite/Cu interfaces varies with the degree of lithiation [20,21], how the ion intercalation affects the ITC be-

<sup>\*</sup> Corresponding authors.

**Table 1** The lithiation degree, number of intercalated Li ions, and atomic charge of the carbon atoms in  $\text{Li}_x\text{C}_6$ . A constant charge of +0.882e is assigned to intercalated Li ions, and the atomic charge of carbon atoms in  $\text{Li}_x\text{C}_6$  is determined accordingly to keep the charge neutrality of simulation systems. The charge densities ( $\sigma$ , calculation details are given in the supplementary materials) on the  $\text{Li}_x\text{C}_6$  basal and edge planes are calculated based on the atomic charge of each carbon atom in  $\text{Li}_x\text{C}_6$ .

Li <sub>x</sub> C <sub>6</sub>	Graphite	LiC <sub>18</sub>	LiC <sub>12</sub>	LiC <sub>10</sub>	LiC <sub>8</sub>	LiC <sub>6</sub>
Lithiation degree	x = 0	x = 1/3	x = 0.5	x = 0.6	x = 0.75	<i>x</i> = 1
Number of Li ions	0	320	480	576	720	960
Charge (e/carbon)	0	-0.049	-0.0735	-0.0882	-0.11025	-0.147
$\sigma_{basal}$ (e/nm <sup>2</sup> )	0	-0.367	-0.55	-0.66	-0.825	-1.1
$\sigma_{edge}$ (e/nm <sup>2</sup> )	0	-0.092	-0.143	-0.172	-0.216	-0.283

tween graphite and polymers remains unknown and deserves further study.

It is known that the intercalated Li ions between adjacent atomic layers can change the interlayer interactions, structures, and atomic charges of the graphite host during the lithiation process [23,24]. These intercalation-induced changes are expected to influence the interactions between graphite basal/edge planes and polymer matrix differently because of the layered structure of graphite, resulting in anisotropic thermal transport across the graphite/polymer interfaces. Although the significance of crossplane ITCs in graphite-based polymeric composites has been highlighted in prior work [25,26], few studies have focused on their in-plane ITCs [11]. In some cases, the in-plane ITC across the graphite/polymer interface is critical for the overall thermal performance of the composites, particularly when edge-enriched materials (e.g., graphitic petals) [27] are involved. Therefore, understanding the effect of Li-ion intercalation on the cross-plane and in-plane interfacial thermal transport between graphite and poly-

In this work, we perform non-equilibrium molecular dynamics (NEMD) simulations to study the thermal transport across Li<sub>x</sub>C<sub>6</sub>/PEO interfaces with different degrees of lithiation. We found that the cross-plane ITC between Li<sub>x</sub>C<sub>6</sub> and PEO monotonically increases with increasing lithiation degrees, while the in-plane ITC between Li<sub>x</sub>C<sub>6</sub> and PEO can only be significantly enhanced when the graphite host is fully lithiated. To understand the underlying mechanisms of such anisotropic ITC enhancements, we investigate the density distribution of PEO, the radial distribution function (RDF) between the two contacting materials, and the vibrational density of state (VDOS) of Li<sub>x</sub>C<sub>6</sub> and PEO to evaluate the atomic interactions and vibrational coupling between LixC6 and PEO at the interface. In addition, we decompose ITC into the contributions from graphite-PEO and Li-PEO interactions, as well as Coulombic and Lenard-Jones (LJ) interactions to evaluate the effect of intercalated Li ions on the thermal transport across Li<sub>x</sub>C<sub>6</sub>/PEO interfaces. The results may provide new insights to the design of thermally conductive polymeric composites and tunable interfaces for more efficient thermal management. The mechanisms revealed in this work may also be applicable to other 2D materials and may provide a better understanding of the thermal transport in polymerbased solid-state lithium-ion batteries.

## 2. Simulation methods

The simulation system consists of 30 P(EO)<sub>50</sub> chains and Li<sub>x</sub>C<sub>6</sub> with an in-plane size of  $\sim 43 \times 45$  Å<sup>2</sup>, which is sufficiently large to include most of the important phonon modes contributing to the interfacial thermal transport and thus can exclude the size effect [11]. The Li<sub>x</sub>C<sub>6</sub> (0  $\leq$  x  $\leq$  1) contains 8 monolayer graphene sheets (720 carbon atoms in each layer) and a corresponding amount of intercalated Li ions (Table 1). The lithiation degree *x* is varied from 0 (pristine graphite) to 1 (fully lithiated graphite, LiC<sub>6</sub>) to repre-

**Table 2** 12-6 Lennard-Jones parameters for Li<sub>x</sub>C<sub>6</sub>.

Interactions	$\varepsilon(\text{kcal/mol})$	σ (Å)	
C-C	0.107496	3.35	
Li-Li	0.025156	2.1835	
C-Li	0.052003	2.76675	

sent different lithiation states of the graphite host (Table 1). In the initial construction of  $Li_xC_6$ , the interlayer spacing is kept at 7 Å, and the Li ions are uniformly placed on the middle plane between two neighboring graphene sheets (Fig. S1). As shown in Fig. 1, the PEO molecules are placed in contact with the Li<sub>x</sub>C<sub>6</sub> basal plane (defined as the 'cross-plane' configuration, Fig. 1a and b) or edge (defined as the 'in-plane' configuration, Fig. 1c and d) to calculate the cross-plane and in-plane ITC values between Li<sub>x</sub>C<sub>6</sub> and PEO, respectively. The force-field parameters of Li<sub>x</sub>C<sub>6</sub> including atomic charges (Table 1) and 12-6 LJ constants (Table 2) are adopted from prior work [19]. In addition, the interactions between the carbon atoms in  $Li_xC_6$  are described by the Tersoff potential. The all-atom optimized potentials for liquid simulation (OPLS-AA) force field, which has been validated in our prior work [14], is employed to model the PEO matrix. The Lorentz-Berthelot mixing rules  $(\varepsilon_{ij} = \operatorname{sqrt}(\varepsilon_i \varepsilon_j); \ \sigma_{ij} = (\sigma_i + \sigma_j)/2$ , where  $\varepsilon$  and  $\sigma$  are the energy and distance constants, respectively) are used to determine the 12-6 LJ parameters for all the intermolecular non-bonding interactions. The long-range Coulombic interaction is evaluated by the particle-particle-mesh (PPPM) algorithm with an accuracy of  $1 \times 10^{-4}$  [28]. Periodic boundary conditions are used in all directions during the relaxation process. A cutoff distance of 10 Å is used for all the non-bonding interactions, including LJ and electrostatic forces. The timestep is set to be 0.25 fs for all simulations because of the light hydrogen atoms [11]. All the molecular structures of  $\text{Li}_x C_6/\text{PEO}$  are visualized by the Open Visualization Tool (OVITO) software [29].

simulations are conducted using the Large-scale Atomic/Molecular Massively Parallel Simulator (LAMMPS) [30]. The interfacial thermal transport between Li<sub>x</sub>C<sub>6</sub> and PEO is evaluated using the NEMD simulation method at 300 K and 1 atm. The simulation system is first relaxed in the isothermal-isobaric (NPT) ensemble at 10 K for 1 ns to stabilize the structure of Li<sub>x</sub>C<sub>6</sub>. The resultant system is annealed to 600 K with a heating rate of 50 K/ns in the NPT ensemble and kept at 600 K for 18 ns to further equilibrate the molecular structures. The system is then quenched to 300 K and equilibrated in the NPT ensemble for 3 ns to converge the density. A final 4 ns of relaxation in the canonical ensemble (NVT) at 300 K is performed before the 4 ns of microcanonical ensemble (NVE) NEMD production simulation. For the  $Li_xC_6/PEO$  interface with the in-plane configuration, a few intercalated Li ions are observed to diffuse into the PEO matrix near the Li<sub>x</sub>C<sub>6</sub>/PEO interface (Fig. S2) during the NPT (600 K) annealing process when the graphite host is not fully lithiated.

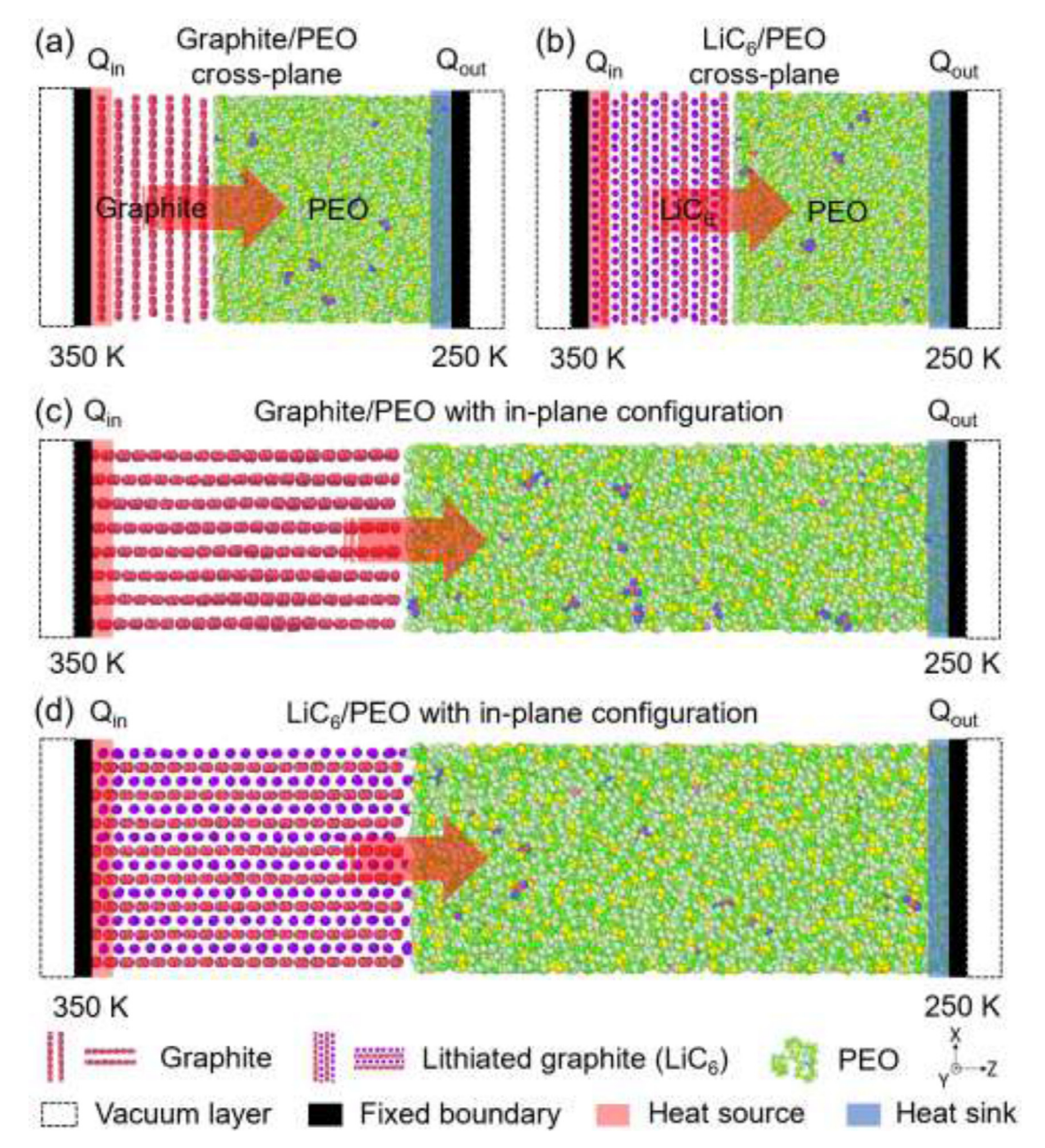


**Fig. 1.** Simulation setup of the representative  $\text{Li}_x\text{C}_6/\text{PEO}$  systems with different interface configurations to calculate the cross-plane and in-plane ITCs: (a) Graphite/PEO system with the cross-plane configuration, (b)  $\text{LiC}_6/\text{PEO}$  system with the cross-plane configuration, (c) Graphite/PEO system with the in-plane configuration, and (d)  $\text{LiC}_6/\text{PEO}$  system with the in-plane configuration. The red arrow shows the heat flow from  $\text{Li}_x\text{C}_6$  to PEO. ITCs are calculated via NEMD simulations: heat source (red) and heat sink (blue) are maintained at 350 K and 250 K using Langevin thermostats, respectively. The two boundaries (black) in the z-direction are fixed by 3 Å. Two 5 Å-thick vacuum layers (areas with black dashed lines) next to these two fixed layers are added to prevent heat leakage between the heat source and heat sink.

These diffusing Li ions are excluded during the NEMD production simulations to avoid their influence on the analysis of thermal transport mechanisms across  $\text{Li}_x \text{C}_6/\text{PEO}$  interfaces.

In the NEMD simulations, the heat source and heat sink are maintained at 350 K and 250 K using Langevin thermostat, respectively. The two boundaries in the z-direction are stabilized by two 3 Å-thick fixed layers. Two 5 Å-thick vacuum layers next to these two fixed layers are added to prevent possible heat leakage between the heat source and heat sink [31]. A slab size of 2 Å, which is less than the width of the interfaces, is used to calculate the temperature profiles in all simulations. ITCs with standard deviations are calculated using the last 2 ns of the production period divided into five time blocks. A relatively large temperature differ-

ence of 100 K between the two thermostats is adopted to improve the signal to noise ratio for calculating the ITC values because the values calculated with a smaller temperature difference of 50 K are within the error bar of the case with a relatively large temperature difference. Fig. 1 shows the representative equilibrated structures of  $\text{Li}_x C_6/\text{PEO}$  (e.g., graphite/PEO,  $\text{LiC}_6/\text{PEO}$ ) systems with the crossplane and in-plane configurations. The corresponding steady-state temperature profiles and energy tallies of these simulation systems are shown in Fig. S3 and S4. After the NEMD simulations reach steady state, ITCs can be calculated from  $G = J/\Delta T$ , where G is the ITC, J is the heat flux, and  $\Delta T$  is the temperature drop across a single  $\text{Li}_x C_6/\text{PEO}$  interface calculated by fitting the temperature profiles at the hot side and cold side (Fig. S3 and S4).

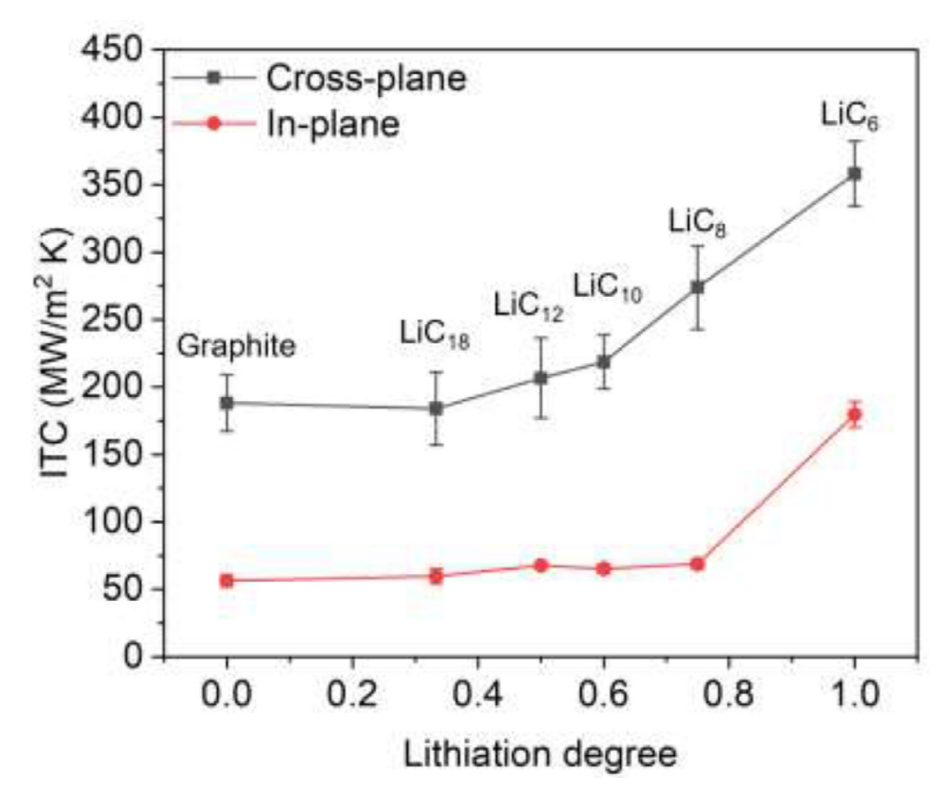


Fig. 2. Cross-plane and in-plane ITCs across the  $Li_xC_6/PEO$  interfaces as a function of lithiation degree x ranging from 0 to 1.

## 3. Results and discussion

## 3.1. Lithiation-controlled ITC between $Li_xC_6$ and PEO

Fig. 2 shows the cross-plane and in-plane ITCs across the Li<sub>x</sub>C<sub>6</sub>/PEO interfaces when the lithiation degree varies from 0 (pristine graphite) to 1 (LiC<sub>6</sub>, fully lithiated graphite). The calculated cross-plane and in-plane ITC values across a single graphite/PEO interface are 188  $\pm$  21  $MW/m^2$  K and 56  $\pm$  4 MW/m<sup>2</sup> K, respectively. These values are comparable to those of the graphene/polymer interfaces, in which the cross-plane and inplane ITCs across two graphene/polymer interfaces fall into the range of 61 - 71 MW/m<sup>2</sup> K (equivalent to 122 - 142 MW/m<sup>2</sup> K for a single interface) and 30 - 32 MW/m<sup>2</sup> K (equivalent to 60 - 64 MW/m<sup>2</sup> K for a single interface), respectively [11]. Moreover, the cross-plane ITC across the Li<sub>x</sub>C<sub>6</sub>/PEO interface increases monotonically with an increasing degree of lithiation (Fig. 2). For instance, the cross-plane ITC across the LiC<sub>6</sub>/PEO interface is 358  $\pm$  24 MW/m<sup>2</sup> K, corresponding to an enhancement of 190% compared with that of the graphite/PEO interface. Comparatively, the in-plane ITC across the  $Li_xC_6/PEO$  interface (Fig. 2) only increases slightly from 56  $\pm$  4 MW/m<sup>2</sup> K to 69  $\pm$  4 MW/m<sup>2</sup> K when the lithiation degree x rises from 0 (graphite) to 0.75 (LiC<sub>8</sub>). A significantly higher in-plane ITC (180  $\pm$  9 MW/m<sup>2</sup> K) is observed when the graphite host is fully lithiated (x = 1, LiC<sub>6</sub>), much higher than those (56 - 69 MW/m<sup>2</sup> K) across other  $Li_xC_6/PEO$  interfaces with the in-plane configuration when  $x \leq 0.75$ . Note that the diffusing Li ions have negligible contributions to the interfacial thermal transport between Li<sub>x</sub>C<sub>6</sub> and PEO with the in-plane configuration. For instance, the ITCs of the LiC<sub>8</sub>/PEO interface with an in-plane configuration with and without the diffusing Li ions are 71  $\pm$  2  $MW/m^2$  K and  $69 \pm 4$   $MW/m^2$  K, respectively. Therefore, these diffusing Li ions (Fig. S2) can be reasonably excluded during the NEMD production simulations.

### 3.2. The density distribution of PEO

When Li ions are intercalated into the graphite host, ionic carbon-lithium bonds will be formed, leading to negatively charged carbon atoms [24]. The electron charges on each carbon atom as a function of lithiation degree are summarized in Table 1. These negatively charged carbon atoms can enhance the Coulombic interactions between Li<sub>x</sub>C<sub>6</sub> and PEO, thus affecting the density distribution of the polymer. Fig. 3 shows the peak densities of PEO near the interfaces in the Li<sub>x</sub>C<sub>6</sub>/PEO systems. The peak densities of PEO near the  $Li_xC_6$  basal plane (cross-plane configuration) or edge plane (in-plane configuration) are generally following a growing trend as the lithiation degree increases. Moreover, the densities of PEO near the Li<sub>x</sub>C<sub>6</sub> basal plane are significantly higher than those near the  $Li_xC_6$  edge plane with the same lithiation degree, which may be attributed to the higher charge density on the Li<sub>x</sub>C<sub>6</sub> basal plane compared with that of the  $Li_xC_6$  edge plane (Table 1). For instance, the peak densities of PEO near the graphite basal and edge planes are 2.1 and 1.48 g/cm<sup>3</sup>, respectively. When the graphite host is fully lithiated ( $LiC_6$ , x = 1), the peak densities of PEO near the LiC<sub>6</sub> basal and edge planes increase to 2.68 and 1.75 g/cm<sup>3</sup>, respectively. Such an observation correlates well with the ITC values shown in Fig. 2, suggesting that the PEO densities at the Li<sub>x</sub>C<sub>6</sub>/PEO interfaces are the key to the enhancement of interfacial thermal transport. Because of the stronger Coulombic interactions between  $Li_xC_6$  and PEO as the lithiation degree increases, more PEO molecules are attracted by Li<sub>x</sub>C<sub>6</sub> closer to its basal plane or edge plane, leading to enhanced cross-plane or in-plane thermal transport across the  $Li_xC_6/PEO$  interfaces.

## 3.3. Radial distribution function (RDF) analysis

Fig. 4 shows the interatomic distances between  $\text{Li}_x\text{C}_6$  and PEO chains near the interfaces with the cross-plane and in-plane con-

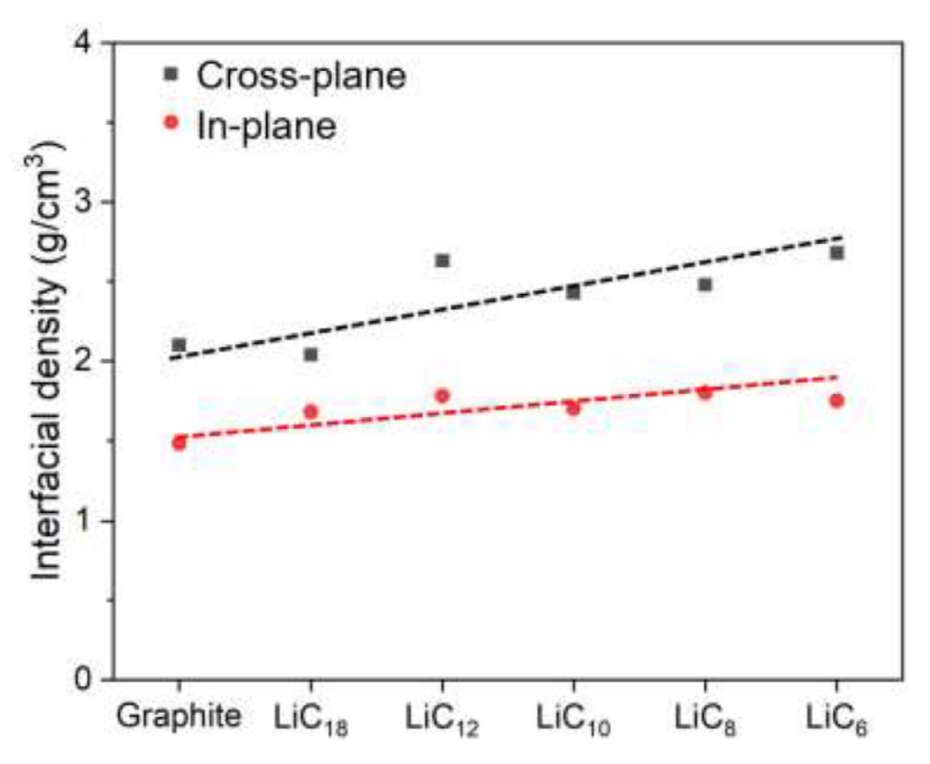


Fig. 3. The peak density of the PEO molecules near Li<sub>x</sub>C<sub>6</sub>/PEO interfaces with different degrees of lithiation.

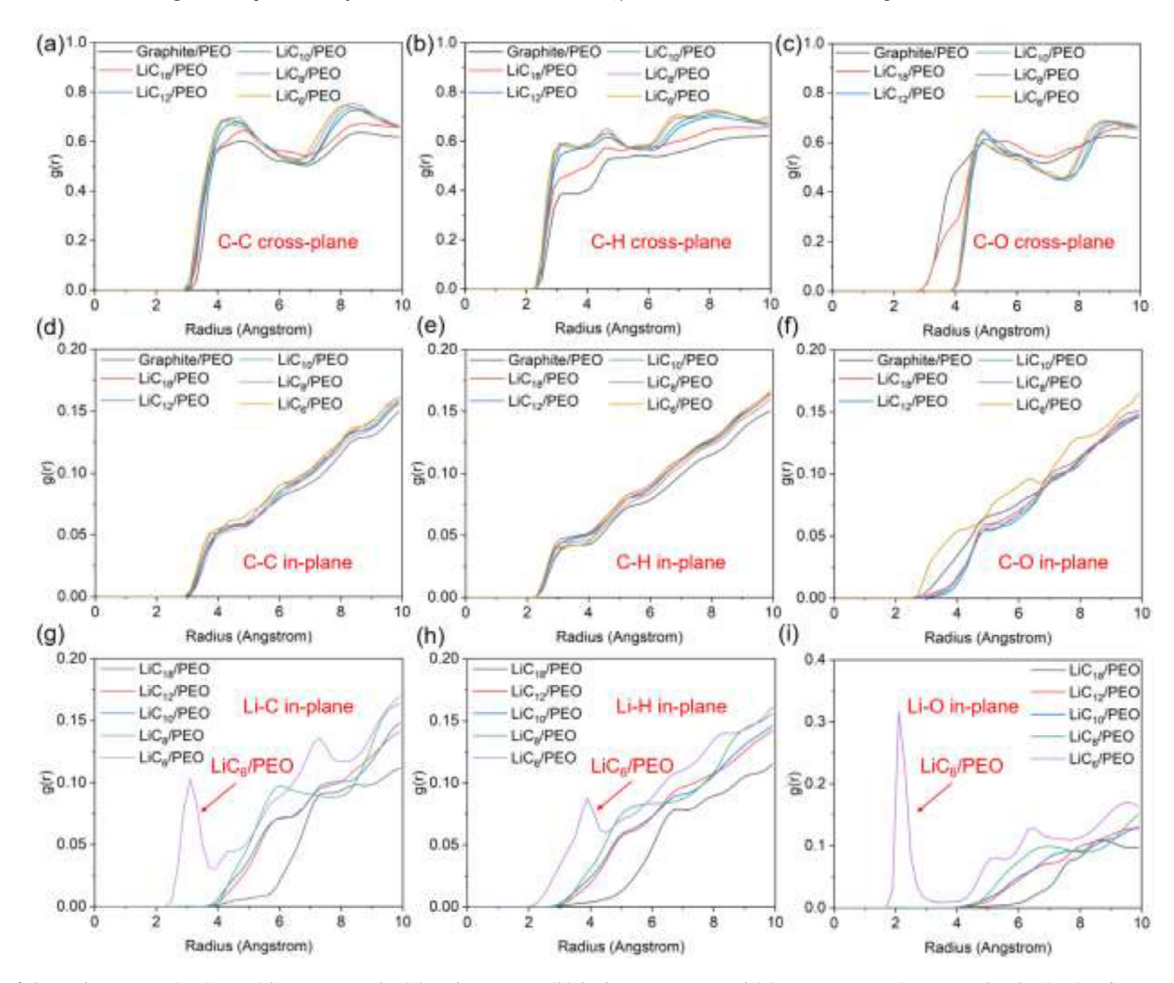


Fig. 4. RDFs of the carbon atoms in  $\text{Li}_x \text{C}_6$  with respect to the (a) carbon atoms, (b) hydrogen atoms, and (c) oxygen atoms in PEO molecules in  $\text{Li}_x \text{C}_6$ /PEO systems with the cross-plane configuration. RDFs of the carbon atoms in  $\text{Li}_x \text{C}_6$  with respect to the (d) carbon atoms, (e) hydrogen atoms, and (f) oxygen atoms in PEO molecules in  $\text{Li}_x \text{C}_6$ /PEO systems with the in-plane configuration. RDFs of the intercalated Li ions in  $\text{Li}_x \text{C}_6$  with respect to the (g) carbon atoms, (h) hydrogen atoms, and (i) oxygen atoms in PEO molecules in  $\text{Li}_x \text{C}_6$ /PEO systems with the in-plane configuration.

figurations. The interatomic distance is characterized by RDF calculated as  $g(r) = n(r)/(4\pi r^2 \rho \Delta r)$ , where n(r) is the number of atoms in a shell of thickness  $\Delta r$  at a distance r from the reference atom in  $Li_xC_6$ , and  $\rho$  is the average atom number density of PEO molecules. To calculate the interatomic distances between  $Li_xC_6$  and PEO, the oxygen (O), carbon (C), or hydrogen (H) atoms are used to represent PEO, and the Li or C atoms are selected to represent Li<sub>x</sub>C<sub>6</sub>. As shown in Fig. 4, the atomic interactions between Li<sub>x</sub>C<sub>6</sub> and PEO differ substantially in the two interfacial configurations. In Li<sub>x</sub>C<sub>6</sub>/PEO systems with the cross-plane configuration, the interatomic distances (indicated by the first peak position of the RDF) between the carbon atoms in  $Li_xC_6$  and the carbon atoms (C-C, Fig. 4a), hydrogen atoms (C-H, Fig. 4b), and oxygen atoms (C-O, Fig. 4c) in PEO molecules are calculated to be 4 Å, 3 Å, and 5 Å, respectively. The C-C and C-H RDFs shift to the left with higher magnitudes (i.e., higher g(r) values) as the lithiation degree increases, indicating that more hydrogen and carbon atoms in the PEO molecules are attracted by the Li<sub>x</sub>C<sub>6</sub> basal plane closer to the interfaces. Such an RDF shift-up phenomenon correlates well with the higher negative charge values of graphite carbon atoms and higher PEO densities at the interfaces as the lithiation degree increases. The more negatively charged carbon atoms lead to a stronger electrostatic attractive force of Li<sub>x</sub>C<sub>6</sub> to PEO molecules and attract these polymer molecules closer to the Li<sub>x</sub>C<sub>6</sub> basal plane, thus increasing the polymer density near the interfaces (Fig. 3a) and providing more pathways for phonon transport. Considering the van der Waals force  $(F_{IJ})$  modeled by 12-6 LJ potential:  $F_{IJ} = -24\varepsilon[2(\frac{\sigma^{12}}{r^{13}}) - (\frac{\sigma^6}{r^7})]$ , where  $\varepsilon$  is the energy constant,  $\sigma$  is the distance constant, and r is the interatomic distance, a shorter interatomic distance can result in a stronger van der Waals force, thus leading to significantly enhanced cross-plane thermal transport across the  $\text{Li}_x \text{C}_6/\text{PEO}$  interfaces particularly at high lithiation degrees (e.g., LiC<sub>8</sub> and LiC<sub>6</sub>), which coincides with the ITC results shown in Fig. 2.

In Li<sub>x</sub>C<sub>6</sub>/PEO systems with the in-plane configuration, the first peak positions of the C-C (Fig. 4d), C-H (Fig. 4e), and C-O (Fig. 4f) RDFs between graphite and PEO are located at 4 Å, 3 Å, and 5 Å, respectively, almost the same as those of the RDFs in Li<sub>x</sub>C<sub>6</sub>/PEO systems with the cross-plane configuration. However, the magnitudes of the RDFs in Li<sub>x</sub>C<sub>6</sub>/PEO systems with the in-plane configuration are much lower than those in Li<sub>x</sub>C<sub>6</sub>/PEO systems with the cross-plane configuration, agreeing well with the density profiles of PEO near the interfaces (Fig. 3a). Furthermore, the RDFs of the C-C (Fig. 4d) and C-H (Fig. 4e) exhibit no significant variations with the lithiation degree in Li<sub>x</sub>C<sub>6</sub>/PEO systems with the in-plane configuration. A noticeable variation is observed for the C-O RDF (Fig. 4f) in the in-plane model when the graphite host is fully lithiated. The results indicate that the oxygen atoms in PEO molecules are attracted closer to LiC<sub>6</sub> edges. To understand such a variation of the C-O RDF in Li<sub>x</sub>C<sub>6</sub>/PEO systems with the in-plane configuration, RDFs of the intercalated Li ions in Li<sub>x</sub>C<sub>6</sub> with respect to the carbon atoms (Li-C, Fig. 4g), hydrogen atoms (Li-H, Fig. 4h), and oxygen atoms (Li-O, Fig. 4i) in PEO molecules are calculated. As shown in Fig. 4i, the first peak position of the Li-O RDF in the LiC<sub>6</sub>/PEO system with the in-plane configuration is significantly decreased to 2.1 Å, which is consistent with the reported Li-O distance between lithium salts and polymer electrolytes (e.g., PEO) in lithium-ion batteries [32,33]. Shorter atomic distances between Li-O atoms lead to stronger interactions between them. It can thus be concluded that the shorter interatomic C-O distance in the LiC<sub>6</sub>/PEO system with the in-plane configuration (Fig. 4f) is induced by the strong Li-O interactions at the interface. Notably, such strong Li-O interactions are only observed in the LiC<sub>6</sub>/PEO system with the in-plane configuration. Therefore, the PEO molecules are attracted closer to the LiC<sub>6</sub> edge plane because of the strong Li-O interactions, which can significantly enhance the in-plane thermal transport between  $\mathrm{LiC}_6$  and  $\mathrm{PFO}$ 

Furthermore, the VDOS of Li<sub>x</sub>C<sub>6</sub> and PEO are analyzed (see details in SI) to quantify the cross-plane and in-plane vibrational coupling effects between the two contacting materials, which can play an important role in interfacial thermal transport [34,35]. The VDOS of Li<sub>x</sub>C<sub>6</sub> (Fig. S5) in the cross-plane and in-plane systems are decomposed to the cross-plane and in-plane vibrational modes, respectively. Although the shift of VDOS is observed in Li<sub>x</sub>C<sub>6</sub> induced by Li-ion intercalation (Fig. S6), the VDOS overlap areas (Table S1) between the cross-plane modes of Li<sub>x</sub>C<sub>6</sub> (Fig. S5a) and PEO (Fig. S7a) in the cross-plane systems remain similar in the frequency range from 0 to 60 THz when lithiation degree varies. The same phenomenon is observed for the VDOS overlap areas between the in-plane modes of Li<sub>x</sub>C<sub>6</sub> (Fig. S5b) and PEO (Fig. S7b) in the in-plane systems. These results imply that the vibrational coupling may exert a minor influence on the thermal transport across Li<sub>x</sub>C<sub>6</sub>/PEO interfaces. Thus, the enhanced ITC may be mainly attributed to the stronger interactions between Li<sub>x</sub>C<sub>6</sub> and PEO induced by Li-ion intercalation, which is different from the phenomena observed in graphite/Al and graphite/Cu systems [20,21].

## 3.4. Decomposition of ITC

To further understand the underlying mechanisms dictating the interfacial thermal transport between Li<sub>x</sub>C<sub>6</sub> and PEO, the crossplane and in-plane ITCs are decomposed into the contributions from graphite-PEO and Li-PEO interactions, as well as LJ and Coulombic interactions (see details in SI), following the methods described in our prior work [14]. As shown in Fig. 5a and b, the cross-plane ITC is mainly contributed by LJ interactions between the graphite host and PEO, while the contributions of Li-PEO and Coulombic interactions to the cross-plane interfacial thermal transport are negligible. Notably, the intercalated Li ions do not directly contribute to the cross-plane interfacial thermal transport across Li<sub>x</sub>C<sub>6</sub>/PEO interfaces because of the long interatomic distance between the intercalated Li ions and PEO molecules, which is consistent with the result reported in prior work (e.g., Li<sub>x</sub>C<sub>6</sub>/Al interface) [20]. These findings suggest that the enhanced long-range Coulombic interactions induced by Li-ion intercalation will attract more PEO molecules closer to the basal planes of Li<sub>x</sub>C<sub>6</sub>, but it is the short-range LJ interactions that dominate and increase the cross-plane interfacial thermal transport across the Li<sub>x</sub>C<sub>6</sub>/PEO interfaces. Such a phenomenon of enhanced thermal transport has been widely observed in other materials in the presence of strong Coulombic interactions [14.16.36].

The LI interactions between graphite host and PEO molecules also dominate the in-plane thermal transport across the Li<sub>x</sub>C<sub>6</sub>/PEO interfaces (Fig. 5c and d) when the graphite host is not fully lithiated. However, the contribution (99.5 MW/m<sup>2</sup> K) of Li-PEO interactions to the in-plane ITC significantly increases and is comparable to that (80.2 MW/m<sup>2</sup> K) of graphite-PEO interactions in LiC<sub>6</sub>/PEO system with the in-plane configuration. Such an observation correlates well with the Li-O RDF in the LiC<sub>6</sub>/PEO system with the in-plane configuration (Fig. 4g-i). Fig. 5e and f show the representative cases of Li<sub>x</sub>C<sub>6</sub>/PEO interfaces with the in-plane configuration when the graphite host is not fully lithiated (e.g.,  $LiC_8/PEO$ , x =0.75) and fully lithiated (LiC<sub>6</sub>/PEO, x = 1), respectively. The intercalated Li ions in LiC<sub>8</sub>/PEO systems with the in-plane configuration are well confined in the LJ gap of the graphite host. Thus, the Li-PEO contributions to the in-plane thermal transport across the LiC<sub>8</sub>/PEO interface are negligible because of the long interatomic distance. However, the densely intercalated Li ions near graphite edges are partially attracted by the PEO molecules in LiC<sub>6</sub>/PEO systems with the in-plane configuration, forming an intermediate Liion layer at the interface (Fig. 5f). These Li ions are confined by

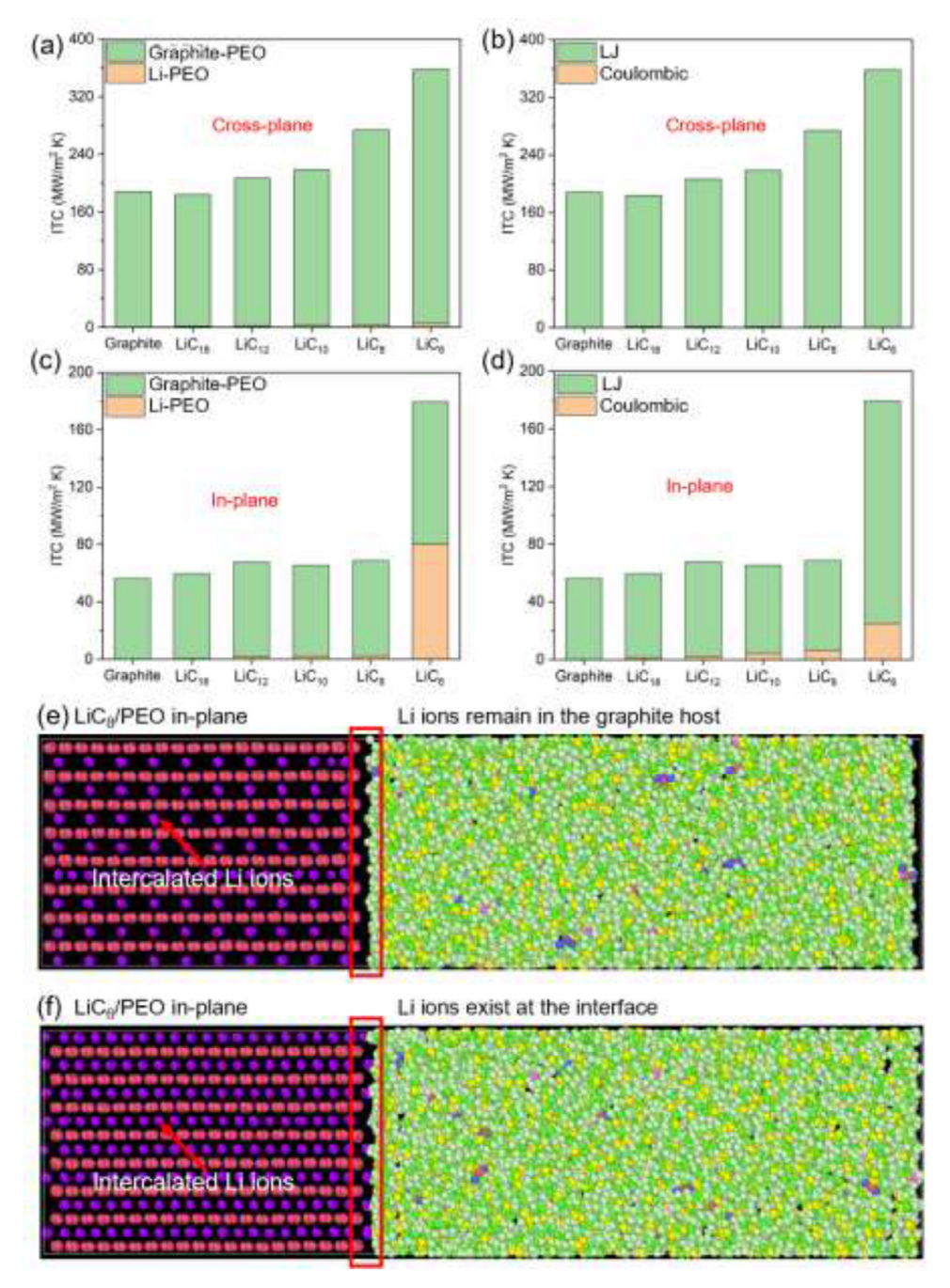


Fig. 5. Decomposition of ITC into different contributions from: (a) graphite-PEO and Li-PEO interactions in the cross-plane systems, (b) LJ and Coulombic interactions in the cross-plane systems, (c) graphite-PEO and Li-PEO interactions in the in-plane systems, and (d) LJ and Coulombic interactions in the in-plane systems. The molecular structures of (e)  $\text{LiC}_8/\text{PEO}$  interface with the in-plane configuration showing the intercalated Li ions are well confined by the graphite host and (f)  $\text{LiC}_6/\text{PEO}$  interface with the in-plane configuration showing the intermediated Li-ion layer at the interface.

the graphite host and cannot diffuse into the PEO matrix. More importantly, this intermediate Li-ion layer leads to short interatomic distances between  $\text{LiC}_6$  and PEO in the in-plane system (Fig. 4d-i). Therefore, the contribution from Li-PEO interaction becomes significant, leading to enhanced in-plane thermal transport across the  $\text{LiC}_6/\text{PEO}$  interface.

#### 4. Conclusions

In summary, we have calculated the cross-plane and in-plane ITCs between  $\text{Li}_x\text{C}_6$  and PEO with different degrees of lithiation. Results show that the interfacial thermal transport between

graphite and PEO in the two directions can be effectively enhanced and controlled by lithiation. The intercalation-induced anisotropic effect on the interfacial thermal conductance between graphite and PEO originates from the layered structure of the graphite host. In the cross-plane case, the intercalated Li ions are well-confined in the graphite host and are isolated from the PEO matrix. While in the in-plane case, an intermediated Li-ion layer between  $\text{Li}_x \text{C}_6$  and PEO can be formed when the graphite host is fully lithiated since the densely intercalated Li ions near the graphite edge are partially attracted by the PEO molecules. We further reveal that the enhanced interfacial thermal transport between  $\text{Li}_x \text{C}_6$  and PEO is mainly contributed by the stronger LJ interactions rather

than Coulombic interactions. When Li ions are intercalated into the graphite host, the strong Coulombic interactions between  $\text{Li}_x \text{C}_6$  and PEO can attract the polymer molecules closer to the basal plane or edge plane of the intercalated graphite host, thus allowing the LJ forces at the interfaces to achieve more efficient thermal transport. The results of this work may provide a novel approach to design controllable 2D material/polymer interfaces and thermally conductive polymeric composites.

#### **Declaration of Competing Interest**

The authors declare that they have no known competing financial interests or personal relationships that could have appeared to influence the work reported in this paper.

### **CRediT authorship contribution statement**

**Siyu Tian:** Investigation, Methodology, Software, Writing – original draft. **Zhihao Xu:** Investigation, Validation, Software. **Shiwen Wu:** Software, Visualization. **Tengfei Luo:** Funding acquisition, Supervision, Writing – review & editing. **Guoping Xiong:** Funding acquisition, Supervision, Writing – review & editing.

#### Acknowledgments

Guoping Xiong acknowledges the financial support from The University of Texas at Dallas startup fund and National Science Foundation (1937949 and 1949962). Tengfei Luo acknowledges the financial support from National Science Foundation (1937923, 1949910, 2001079 and 2040565). The authors acknowledge the Texas Advanced Computing Center (TACC) at The University of Texas at Austin for providing computing resources that have contributed to the research results reported within this paper. URL: http://www.tacc.utexas.edu

## Supplementary materials

Supplementary material associated with this article can be found, in the online version, at doi:10.1016/j.ijheatmasstransfer. 2022.123134.

#### References

- J. Khan, S.A. Momin, M. Mariatti, A review on advanced carbon-based thermal interface materials for electronic devices, Carbon 168 (2020) 65– 112.
- [2] X. Lin, X. Zhang, L. Liu, J. Liang, W. Liu, Polymer/expanded graphite-based flexible phase change material with high thermal conductivity for battery thermal management, J. Clean. Prod. 331 (2022) 130014.
- [3] B. Wei, L. zhang, S. Yang, Polymer composites with expanded graphite network with superior thermal conductivity and electromagnetic interference shielding performance, Chem. Eng. J. 404 (2021) 126437.
- [4] X. Wei, Z. Wang, Z. Tian, T. Luo, Thermal transport in polymers: a review, J. Heat Transf. 143 (7) (2021) 072101.
- [5] C. Huang, X. Qian, R. Yang, Thermal conductivity of polymers and polymer nanocomposites, Mater. Sci. Eng. R Rep. 132 (2018) 1–22.
- [6] N. Mehra, L. Mu, T. Ji, X. Yang, J. Kong, J. Gu, J. Zhu, Thermal transport in polymeric materials and across composite interfaces, Appl. Mater. Today 12 (2018) 92–130
- [7] X. Wan, D. Ma, D. Pan, L. Yang, N. Yang, Optimizing thermal transport in graphene nanoribbon based on phonon resonance hybridization, Mater. Today Phys. 20 (2021) 100445.
- [8] S. Deng, J. Yuan, Y. Lin, X. Yu, D. Ma, Y. Huang, G. Zhang, N. Yang, Electric-field-induced modulation of thermal conductivity in poly(vinylidene fluoride), Nano Energy 82 (2021) 105749.
- [9] S. Deng, D. Ma, G. Zhang, N. Yang, Modulating the thermal conductivity of crystalline nylon by tuning hydrogen bonds through structure poling, J. Mater. Chem. A 9 (43) (2021) 24472–24479.

- [10] X. Wan, B. Demir, M. An, T.R. Walsh, N. Yang, Thermal conductivities and mechanical properties of epoxy resin as a function of the degree of cross-linking, Int. J. Heat Mass Transf. 180 (2021) 121821.
- [11] T. Luo, J.R. Lloyd, Enhancement of thermal energy transport across graphene/graphite and polymer interfaces: a molecular dynamics study, Adv. Funct. Mater. 22 (12) (2012) 2495–2502.
- [12] L. Yang, X. Wan, D. Ma, Y. Jiang, N. Yang, Maximization and minimization of interfacial thermal conductance by modulating the mass distribution of the interlayer, Phys. Rev. B 103 (15) (2021) 155305.
- [13] W. Ren, Y. Ouyang, P. Jiang, C. Yu, J. He, J. Chen, The impact of interlayer rotation on thermal transport across graphene/hexagonal boron nitride van der waals heterostructure, Nano Lett. 21 (6) (2021) 2634–2641.
- [14] S. Tian, D. Huang, Z. Xu, S. Wu, T. Luo, G. Xiong, Enhanced thermal transport across the interface between charged graphene and poly(ethylene oxide) by non-covalent functionalization, Int. J. Heat Mass Transf. 183 (2022) 122188.
- [15] Y. Guo, D. Surblys, H. Matsubara, T. Ohara, A molecular dynamics study of the effect of functional groups and side chain on adsorption of alcoholic surfactant and interfacial thermal transport, J. Mol. Liq. 335 (2021) 116243.
- [16] T. Zhang, A.R. Gans-Forrest, E. Lee, X. Zhang, C. Qu, Y. Pang, F. Sun, T. Luo, Role of hydrogen bonds in thermal transport across hard/soft material interfaces, ACS Appl. Mater. Interfaces 8 (48) (2016) 33326–33334.
- [17] G. Zhu, J. Liu, Q. Zheng, R. Zhang, D. Li, D. Banerjee, D.G. Cahill, Tuning thermal conductivity in molybdenum disulfide by electrochemical intercalation, Nat. Commun. 7 (1) (2016) 13211.
- [18] J.S. Kang, M. Ke, Y. Hu, Ionic intercalation in two-dimensional van der waals materials: in situ characterization and electrochemical control of the anisotropic thermal conductivity of black phosphorus, Nano Lett. 17 (3) (2017) 1431–1438.
- [19] X. Qian, X. Gu, M.S. Dresselhaus, R. Yang, Anisotropic tuning of graphite thermal conductivity by lithium intercalation, J. Phys. Chem. Lett. 7 (22) (2016) 4744–4750
- [20] Z. Wei, W. Ju, K. Bi, J. Yang, Y. Chen, Significant enhancement of thermal boundary conductance in graphite/Al interface by ion intercalation, Int. J. Heat Mass Transf. 157 (2020) 119946.
- [21] Z. Wei, F. Yang, K. Bi, J. Yang, Y. Chen, Tuning the interfacial thermal conductance via the anisotropic elastic properties of graphite, Carbon 144 (2019) 109–115.
- [22] R. Bhattacharyya, B. Key, H. Chen, A.S. Best, A.F. Hollenkamp, C.P. Grey, *In situ* NMR observation of the formation of metallic lithium microstructures in lithium batteries, Nat. Mater. 9 (6) (2010) 504–510.
- [23] B. Wang, L.W. Le Fevre, A. Brookfield, E.J.L. McInnes, R.A.W. Dryfe, Resolution of lithium deposition versus intercalation of graphite anodes in lithium ion batteries: an *in situ* electron paramagnetic resonance study, Angew. Chem. Int. Ed. 60 (40) (2021) 21860–21867.
- [24] J.P. Ritchie, S.M. Bachrach, Bond paths and bond properties of carbon-lithium bonds, J. Am. Chem. Soc. 109 (20) (1987) 5909–5916.
- [25] Y. Gao, F. Müller-Plathe, Increasing the thermal conductivity of graphene-polyamide-6,6 nanocomposites by surface-grafted polymer chains: calculation with molecular dynamics and effective-medium approximation, J. Phys. Chem. B 120 (7) (2016) 1336–1346.
- [26] Y. Wang, C. Yang, Q.X. Pei, Y. Zhang, Some aspects of thermal transport across the interface between graphene and epoxy in nanocomposites, ACS Appl. Mater. Interfaces 8 (12) (2016) 8272–8279.
- [27] A. Kumar, N. Ayyagari, T.S. Fisher, Effects of graphene nanopetal outgrowths on internal thermal interface resistance in composites, ACS Appl. Mater. Interfaces 8 (10) (2016) 6678–6684.
- [28] R.W.E. Hockney, Computer Simulation using Particles J. W., Taylor & Francis, Inc, 1988.
- [29] A. Stukowski, Visualization and analysis of atomistic simulation data with OVI-TO-the open visualization tool, Modell. Simul. Mater. Sci. Eng. 18 (1) (2009) 015012
- [30] S.C. Plimpton, A. Thompson, LAMMPS-large-scale atomic/molecular massively parallel simulator, Sandia Natl. Lab. (2007) http://Lammps.Sandia.Gov.
- [31] S. Begić, E. Jónsson, F. Chen, M. Forsyth, Molecular dynamics simulations of pyrrolidinium and imidazolium ionic liquids at graphene interfaces, Phys. Chem. Chem. Phys. 19 (44) (2017) 30010–30020.
- [32] M.A. Webb, Y. Jung, D.M. Pesko, B.M. Savoie, U. Yamamoto, G.W. Coates, N.P. Balsara, Z.-G. Wang, T.F. Miller, Systematic computational and experimental investigation of lithium-ion transport mechanisms in polyester-based polymer electrolytes, ACS Cent. Sci. 1 (4) (2015) 198–205.
- [33] Q. Zheng, D.M. Pesko, B.M. Savoie, K. Timachova, A.L. Hasan, M.C. Smith, T.F. Miller, G.W. Coates, N.P. Balsara, Optimizing ion transport in polyether-based electrolytes for lithium batteries, Macromolecules 51 (8) (2018) 2847–2858.
- [34] Z. Xu, D. Huang, T. Luo, Molecular-level understanding of efficient thermal transport across the silica-water interface, J. Phys. Chem. C 125 (43) (2021) 24115–24125.
- [35] T. Luo, G. Chen, Nanoscale heat transfer from computation to experiment, Phys. Chem. Chem. Phys. 15 (10) (2013) 3389–3412.
- [36] X. Wei, T. Luo, Role of ionization in thermal transport of solid polyelectrolytes, J. Phys. Chem. C 123 (20) (2019) 12659–12665.